Electrocatalysis

International Edition: DOI: 10.1002/anie.201609080
German Edition: DOI: 10.1002/ange.201609080

Engineering the Electrical Conductivity of Lamellar Silver-Doped Cobalt(II) Selenide Nanobelts for Enhanced Oxygen Evolution

Xu Zhao, Hantao Zhang, Yu Yan, Jinhua Cao, Xingqi Li, Shiming Zhou, Zhenmeng Peng, and Jie Zeng**

Abstract: *Precisely engineering the electrical conductivity represents a promising strategy to design efficient catalysts towards oxygen evolution reaction (OER). Here, we demonstrate a versatile partial cation exchange method to fabricate lamellar Ag-$CoSe_2$ nanobelts with controllable conductivity. The electrical conductivity of the materials was significantly enhanced by the addition of Ag^+ cations of less than 1.0 %. Moreover, such a trace amount of Ag induced a negligible loss of active sites which was compensated through the effective generation of active sites as shown by the excellent conductivity. Both the enhanced conductivity and the retained active sites contributed to the remarkable electrocatalytic performance of the Ag-$CoSe_2$ nanobelts. Relative to the $CoSe_2$ nanobelts, the as-prepared Ag-$CoSe_2$ nanobelts exhibited a higher current density and a lower Tafel slope towards OER. This strategy represents a rational design of efficient electrocatalysts through finely tuning their electrical conductivities.*

The oxygen evolution reaction (OER) has received growing attention because of its wide application in energy conversion and storage, such as hydrogen production from water splitting, regenerative fuel cells, and rechargeable metal–air batteries.[1–4] However, OER suffers from intrinsically sluggish kinetics because of the involvement of multiple proton-coupled electron-transfer steps.[5] Although precious metal oxides such as IrO_2 and RuO_2 are generally employed as active electrocatalysts to facilitate the sluggish kinetics, their low abundance and high costs significantly make it impractical to commercialize these electrocatalysts.[6] Accordingly, it is attractive to develop alternative OER electrocatalysts made of earth-abundant elements, such as the 3d transition metals and their derivatives.[7–9] Notably, $CoSe_2$ can be regarded as an alternative catalyst owing to its $t_{2g}^6e_g^1$ electronic configuration, close to an optimal e_g filling for OER.[10] In order to optimize the electrocatalytic performance of $CoSe_2$, great efforts have been made to develop strategies, such as creating electronic interactions by, for example, constructing hybrid structures with metals or metal oxides, and increasing the number of active sites by reducing the thickness at atomic scale.[11–14] Proper electrical conductivity serves as a prerequisite for catalysts with remarkable electrocatalytic performance. A high electrical conductivity ensures a fast electron-transfer process to reduce the Schottky barriers at both catalyst–electrolyte and catalyst–electrode interfaces.[15] Therefore, it is of significant importance to precisely engineer the intrinsic electrical conductivity of $CoSe_2$-based catalysts.

As a versatile chemical transformation method, the cation exchange reaction can be employed to modify composition, structure, and properties of nanomaterials through replacing the existing cations in the crystal lattice with other cations.[16–18] For instance, Zhang and co-workers have demonstrated a selective cation exchange reaction to prepare $Cd_xZn_{1-x}Se$ nanoframes with improved photocatalytic properties towards hydrogen evolution from water splitting.[19] In addition, porous CuS/ZnS nanosheets as an active visible-light-driven photocatalyst were prepared through a simple cation exchange reaction between ZnS nanosheets and $Cu(NO_3)_2$.[20] Particularly, the cation exchange reaction represents an effective approach for modification of metal chalcogenides, because the mobility of metal cations in the anionic framework allows for the replacement of cations under moderate reaction conditions.[21]

Herein, we apply a facile partial cation exchange method to prepare lamellar Ag-$CoSe_2$ nanobelts with controllable electrical conductivity for enhanced OER activity. The introduction of Ag^+ cations of less than 1.0 % could enhance the conductivity of the Ag-$CoSe_2$ nanobelts. Benefiting from the enhanced conductivity and the retained active sites, the as-prepared Ag-$CoSe_2$ nanobelts exhibited a remarkable activity towards OER. The OER overpotential of Ag-$CoSe_2$ nanobelts was 0.32 V at a current density of 10 $mA\,cm^{-2}$, which was lower than that of $CoSe_2$ nanobelts. Moreover, Ag-$CoSe_2$ nanobelts showed a high current density of 22.36 $mA\,cm^{-2}$ at an overpotential of 0.35 V and a small Tafel slope of 56 $mV\,dec^{-1}$ relative to the $CoSe_2$ nanobelts. In addition, a superior stability was also demonstrated for the Ag-$CoSe_2$ nanobelts after long-term potential cycles.

To begin with, $CoSe_2$-diethylenetriamine ($CoSe_2$-DETA) nanobelts were synthesized via a facile amine-assisted solvothermal method.[22] As shown in Figure S1 in the Support-

[*] X. Zhao, H. Zhang, Y. Yan, J. Cao, X. Li, S. Zhou, Prof. J. Zeng
Hefei National Laboratory for Physical Sciences at the Microscale
Key Laboratory of Strongly-Coupled Quantum Matter Physics of Chinese Academy of Sciences, Hefei Science Center
National Synchrotron Radiation Laboratory
Department of Chemical Physics
University of Science and Technology of China
Hefei, Anhui 230026 (P.R. China)
E-mail: zengj@ustc.edu.cn
Prof. Z. Peng
Department of Chemical and Biomolecular Engineering
University of Akron
Akron, OH 44325 (USA)
E-mail: zpeng@uakron.edu

Supporting information for this article can be found under: http://dx.doi.org/10.1002/anie.201609080.

ing Information, smooth and flexible $CoSe_2$-DETA nanobelts were successfully prepared in high purity. The X-ray diffraction (XRD) pattern of $CoSe_2$ was indexed as a pure primitive cubic phase (JCPDS No.09-234). The as-prepared $CoSe_2$-DETA nanobelts were then added into an aqueous solution containing an appropriate amount of $AgNO_3$. The resultant lamellar Ag-$CoSe_2$ nanobelts were obtained after the reaction had proceeded at 160 °C for 6 h. Figure 1 A shows the typical

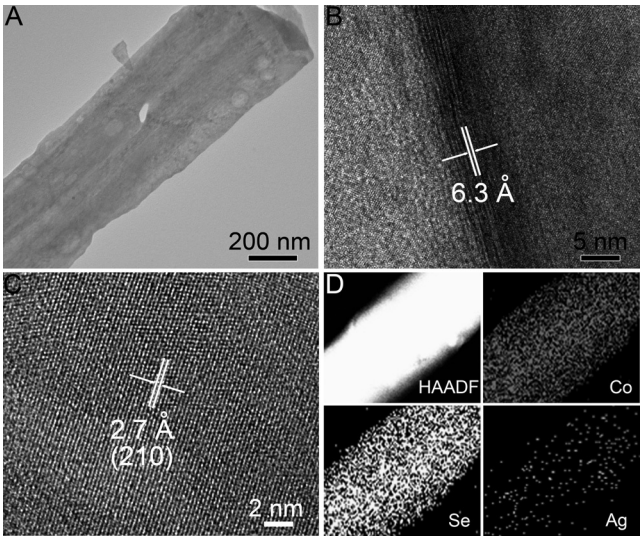

Figure 1. A) TEM image of 1.0% Ag-$CoSe_2$ nanobelts. B, C) HRTEM image of 1.0% Ag-$CoSe_2$ nanobelts. D) HAADF-STEM image and STEM-EDX elemental mapping images of Co, Se, and Ag in 1.0% Ag-$CoSe_2$ nanobelts.

transmission electron microscopy (TEM) image of Ag-$CoSe_2$ nanobelts. Apparently, the smooth, ultrathin, and belt-like structures with widths of 300–500 nm were basically retained for Ag-$CoSe_2$ nanobelts after the cation exchange treatment. Moreover, several irregular voids were observed on the surface of the Ag-$CoSe_2$ nanobelts, mainly owing to rapid kinetics and strain release induced by the large lattice mismatch between Ag and Co.[23] To further visualize the structure of Ag-$CoSe_2$ nanobelts, high-resolution TEM (HRTEM) images are provided in Figure 1, B and C. The sample took the morphology of highly ordered lamellar nanobelts with the interlayer distance of 6.3 Å. The periodic lattice fringes reveal the single-crystal characteristic of Ag-$CoSe_2$ nanobelts. The lattice spacing of 2.7 Å was assigned to (210) planes of $CoSe_2$ in the cubic phase. In the absence of Ag, $CoSe_2$ nanobelts showed no observable changes in the lattice spacing and interlayer distance relative to that of Ag-$CoSe_2$ nanobelts, indicating that the structure was well retained after the cation exchange process (Figure S2). Figure 1 D presents a high-angle annular dark-field scanning TEM (HAADF-STEM) and its corresponding elemental mapping images of the Ag-$CoSe_2$ nanobelts. The results clearly demonstrate the homogeneously distribution of Co, Se and Ag. From the energy dispersive X-ray (EDX) spectrum in Figure S3, besides signals for Co and Se, the signal for Ag was also clearly observed, further confirming the successful introduction of Ag^+ cations. The concentration of Ag^+ ions in the sample was determined as 1.0% by inductively coupled plasma-atomic emission spectroscopy (ICP-AES) analysis, as such we denoted the sample as 1.0% Ag-$CoSe_2$ nanobelts. By simply varying the amounts of Ag^+ cations added, similar ultrathin nanobelts with Ag molar ratio of 0.02% and 0.1% were successfully prepared, which were denoted as 0.02% Ag-$CoSe_2$ and 0.1% Ag-$CoSe_2$ nanobelts, respectively (Figure S4).

The XRD patterns of all the Ag-$CoSe_2$ nanobelts were similar to that of $CoSe_2$ in a primitive cubic phase (Figure 2 A), indicating negligible changes of the crystalline structures after the introduction of Ag^+ cations. The disappearance of several reflections should be related to the

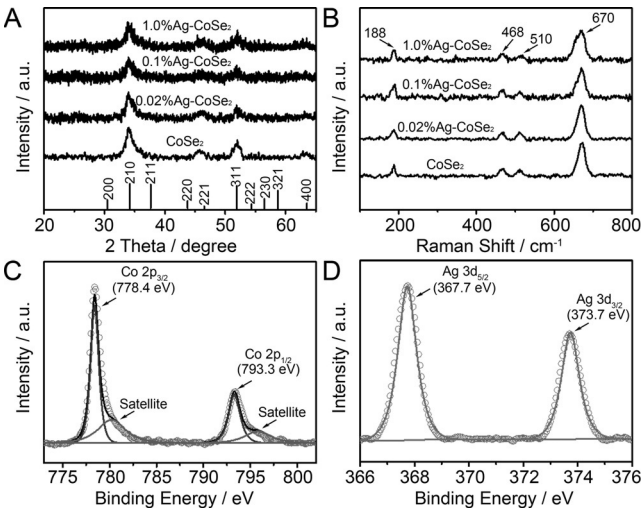

Figure 2. A) XRD patterns of 0.02% Ag-$CoSe_2$, 0.1% Ag-$CoSe_2$, 1.0% Ag-$CoSe_2$, and $CoSe_2$ nanobelts. The standard diffraction peaks of pure $CoSe_2$ (JCPDS No.09-234) are attached at the bottom for comparison. B) Raman spectra of Ag-$CoSe_2$ nanobelts. C) Co 2p XPS and D) Ag 3d XPS spectra of 1.0% Ag-$CoSe_2$ nanobelts.

ultrathin, layered structure of the nanobelts.[22] In addition, the preferred (210) orientation is consistent with the selected growth direction in the HETEM of the 1.0% Ag-$CoSe_2$ nanobelts. Figure 2 B shows the Raman spectra of the Ag-$CoSe_2$ nanobelts. Four typical Raman peaks located at 188, 468, 510 and 670 cm^{-1} were found for Ag-$CoSe_2$ nanobelts, corresponding to those of the cubic $CoSe_2$ structure.[24,25] In addition, the full-width at half-maximum (FWHM) at 670 cm^{-1} increased with Ag introduction (Figure S5), implying the structural disorder caused by the introduction of Ag^+ cations.[26] For first-row metal dichalcogenides, it is known that the low-spin, divalent metal cations are octahedrally coordinated with S_2^{2-} or Se_2^{2-} dimers.[27] To gain further insight into the valence state of the as-prepared 1.0% Ag-$CoSe_2$ nanobelts, X-ray photoelectron spectroscopy (XPS) analysis was carried out. As shown in Figure 2 C, the binding energies of Co $2p_{3/2}$ at 778.4 eV and Co $2p_{1/2}$ at 793.4 eV corresponded to Co^{2+} cations in $CoSe_2$. Notably, obvious shake-up satellites were found at the higher energy side of the Co 2p signal, indicating the antibonding orbital between the

Co and Se atom.[28–31] Figure 2D shows the binding energy of Ag $3d_{5/2}$ peak at 367.7 eV, which can be assigned to Ag^+ cations in Ag_2Se, confirming the occurrence of cation exchange reaction between $CoSe_2$ nanobelts and Ag^+ cations.[32]

The electrocatalytic OER properties of lamellar Ag-$CoSe_2$ nanobelts with different Ag molar ratios were evaluated in O_2-saturated 0.1 M KOH solution using a standard three-electrode system. The catalysts were uniformly cast onto a glassy carbon electrode with a total loading of 200 $\mu g\,cm^{-2}$. For comparison, similar measurements were also carried out for $CoSe_2$ nanobelts. Figure 3A shows

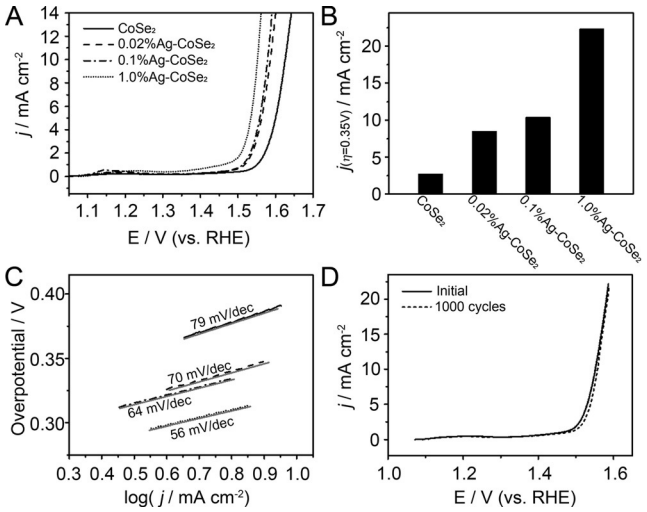

Figure 3. A) IR-corrected polarization curves of Ag-$CoSe_2$ and $CoSe_2$ nanobelts in O_2-saturated 0.1 M KOH solution. B) Current densities of Ag-$CoSe_2$ and $CoSe_2$ nanobelts at an overpotential of 0.35 V. C) Tafel plots of Ag-$CoSe_2$ and $CoSe_2$ nanobelts. D) OER polarization curves of 1.0% Ag-$CoSe_2$ nanobelts before and after potential sweeps of 1000 cycles.

polarization curves recorded by linear sweep voltammetry at a slow scan rate of 5 $mV\,s^{-1}$ with a continuous rotating speed of 1600 rpm. The ohmic potential drop (iR) losses caused by electrolyte resistance were all corrected before comparison. Remarkably, relative to $CoSe_2$ nanobelts, all of the Ag-$CoSe_2$ nanobelts exhibited lower onset potentials and higher current densities. Among all of the tested catalysts, 1.0% Ag-$CoSe_2$ nanobelts exhibited the lowest overpotential of 0.32 V at the current density of 10 $mA\,cm^{-2}$, which represents a metric relevant to the production of solar fuels.[33] Notably, the introduction of Ag^+ induced negligible variation of the pre-OER oxidation peak assigned to the Co^{II} to Co^{III} transition for active sites generation, indicating that the active sites were retained. To directly compare the electrocatalytic performance of all the catalysts, the current densities at a fixed overpotential of 0.35 V were summarized in Figure 3B. The 1.0% Ag-$CoSe_2$ nanobelts showed the highest current density of 22.36 $mA\,cm^{-2}$, which was 8.2, 2.6, and 2.1 times as high as that of $CoSe_2$, 0.02% Ag-$CoSe_2$, and 0.1% Ag-$CoSe_2$ nanobelts, respectively. Given the proportional relationship between the current density and the yield of oxygen, 1.0% Ag-$CoSe_2$ nanobelts exhibited the highest OER activity. Meanwhile, the corresponding Tafel plots shown in Figure 3C for 1.0% Ag-$CoSe_2$ nanobelts exhibited a relatively lower Tafel slope of 56 mV/dec than that for the $CoSe_2$ nanobelts (79 mV/dec), implying significantly accelerated OER kinetics owing to the involvement of Ag^+ cations. To gain further insight into the OER kinetics of these Ag-$CoSe_2$ nanobelts, electrical impedance spectroscopy (EIS) analysis was carried out. Figure S6A shows the Nyquist plots of Ag-$CoSe_2$ nanobelts with different Ag ratios. The semicircle diameter in the high frequency range of the Nyquist plot is associated with the charge transfer resistance (R_{ct}). R_{ct} decreased from 50.3 to 39.6 Ω with the increase of Ag atomic percentage from 0.02% to 1.0%, indicating the improved charge transfer kinetics with the increase of Ag^+ cations (Figure S6B). Notably, the OER activity of 1.0% Ag-$CoSe_2$ nanobelts was higher than those of recently reported Co-based catalysts (Table S1). In addition, continuous potential cycling in O_2-saturated 0.1 M KOH solution was carried out to access the OER stability of 1.0% Ag-$CoSe_2$ nanobelts. As shown in Figure 3D, a negligible variation in the activity was observed after 1000 potential cycles. The Ag concentration of the 1.0% Ag-$CoSe_2$ after OER tests was measured to be 0.8%, indicating only a slight decrease and suggesting a good stability of the structure. The good stability of the 1.0% Ag-$CoSe_2$ was further confirmed by the imperceptible structural variation observed with TEM and XRD characterizations (Figure S7).

Considering that high conductivity could facilitate the charge transfer process, the remarkable electrocatalytic activity of Ag-$CoSe_2$ nanobelts is likely to derive from their enhanced conductivity induced by the introduction of Ag. To investigate the influence of the introduction of Ag^+ cations on the electrical conductivity of Ag-$CoSe_2$ nanobelts, measurements of the temperature dependent resistivity of the 1.0% Ag-$CoSe_2$ and $CoSe_2$ nanobelts were carried out. As shown in Figure 4A, the electrical resistivity of the 1.0% Ag-$CoSe_2$ and

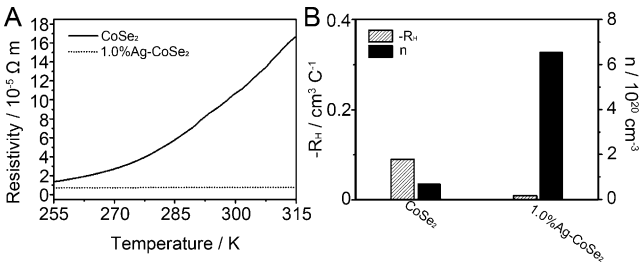

Figure 4. A) Temperature-dependent electrical resistivity of 1.0% Ag-$CoSe_2$ and $CoSe_2$ nanobelts. B) Hall coefficient (R_H) and carrier concentration (n) of 1.0% Ag-$CoSe_2$ and $CoSe_2$ nanobelts at 300 K.

$CoSe_2$ nanobelts both increased with the elevated temperature, showing $d\rho/dT > 0$. This result indicates that both the samples exhibited a typical metallic behavior. Moreover, the corresponding electrical resistivity of $7.48 \times 10^{-6}\,\Omega m$ for 1.0% Ag-$CoSe_2$ nanobelts at 300 K was significantly lower than that of $1.05 \times 10^{-4}\,\Omega m$ for $CoSe_2$ nanobelts, indicating the improved conductivity after the addition of Ag^+ cations.

The Hall coefficient (R_H) was further measured to compare the charge transport properties of 1.0% Ag-$CoSe_2$ and $CoSe_2$ nanobelts. As illustrated in Figure 4B, both the samples show negative R_H at 300 K, indicating that their charge carriers are electrons. The carrier concentration (n) derived from the Hall coefficient for 1.0% Ag-$CoSe_2$ shows an increase by 9.5 times at 300 K compared with that for $CoSe_2$ nanobelts, which further confirms the improved conductivity of 1.0% Ag-$CoSe_2$ nanobelts.

The enhanced conductivity and high carrier concentration induced by the introduction of Ag^+ cations could facilitate the charge transfer process that serves as the key step in electrocatalysis, thereby making Ag-$CoSe_2$ nanobelts an ideal catalyst for OER. Previous mechanistic studies have discovered that the real active sites of Co-based OER catalyst are the Co^{IV}. These active sites are generated in situ prior to OER process through a typical oxidation process, in which Co^{II} is oxidized to Co^{III} and Co^{IV}.[34] Specific to the Ag-$CoSe_2$ catalyst in this study, the generation of surface active sites could be facilitated owing to significantly improved electron transport, leading to more Co^{IV} sites and consequently promoted OER rate. On the other side, the cation exchange between Co^{2+} and Ag^+ could negatively influence the Co^{IV} generation considering a fraction of Co^{2+} being replaced by Ag^+. We measured electrochemical active surface area (ECSA), which is representative of Co^{2+} amount, of the catalysts for examining this effect. Only a 5.6% decrease in ECSA was observed after the introduction of trace amount of Ag cations (below 1.0%) (Figure S8), suggesting the Co^{2+} loss in the Ag-$CoSe_2$ is minimal. The small loss in Co^{2+} sites could be compensated through their more effective generation of Co^{IV} active sites. Collectively, both the enhanced conductivity and retained active sites contributed to the remarkable electrocatalytic performance of Ag-$CoSe_2$ nanobelts.

In conclusion, we have successfully engineered the electrical conductivity of lamellar Ag-$CoSe_2$ nanobelts using a partial cation exchange method. The addition of a trace amount of Ag^+ cations could enhance the conductivity of Ag-$CoSe_2$ nanobelts while retaining the active sites, therefore rendering Ag-$CoSe_2$ nanobelts an efficient OER electrocatalyst. We believe that this work paves a novel pathway for designing highly efficient OER catalysts based on the modification of electrical conductivity. Moreover, this strategy is promising to be extended to the applications in energy storage and conversion.

Acknowledgements

This work was supported by Collaborative Innovation Center of Suzhou Nano Science and Technology, MOST of China (grant number 2014CB932700), NSFC under grant numbers 21573206, 51371164, and 51132007, Key Research Program of Frontier Sciences of the CAS (QYZDB-SSW-SLH017), Strategic Priority Research Program B of the CAS under grant number XDB01020000, Hefei Science Center CAS (2015HSC-UP016), and Fundamental Research Funds for the Central Universities. We also thank the National Synchrotron Radiation Laboratory (BL10B, NSRL) for help in characterizations.

Keywords: cation exchange reaction · electrical conductivity · electrocatalysis · nanostructures · oxygen evolution reaction

How to cite: *Angew. Chem. Int. Ed.* **2017**, *56*, 328–332
Angew. Chem. **2017**, *129*, 334–338

[1] A. Grimaud, K. J. May, C. E. Carlton, Y.-L. Lee, M. Risch, W. T. Hong, J. G. Zhou, Y. Shao-Horn, *Nat. Commun.* **2013**, *4*, 2439.
[2] R. Subbaraman, D. Tripkovic, K.-C. Chang, D. Strmcnik, A. P. Paulikas, P. Hirunsit, M. Chan, J. Greeley, V. Stamenkovic, N. M. Markovic, *Nat. Mater.* **2012**, *11*, 550.
[3] I. Katsounaros, S. Cherevko, A. R. Zeradjanin, K. J. J. Mayrhofer, *Angew. Chem. Int. Ed.* **2014**, *53*, 102; *Angew. Chem.* **2014**, *126*, 104.
[4] Z.-L. Wang, D. Xu, J.-J. Xu, X.-B. Zhang, *Chem. Soc. Rev.* **2014**, *43*, 7746.
[5] P. Z. Chen, K. Xu, T. P. Zhou, Y. Tong, J. C. Wu, H. Cheng, X. L. Lu, H. Ding, C. Z. Wu, Y. Xie, *Angew. Chem. Int. Ed.* **2016**, *55*, 2488; *Angew. Chem.* **2016**, *128*, 2534.
[6] T. Maiyalagan, K. A. Jarvis, S. Therese, P. J. Ferreira, A. Manthiram, *Nat. Commun.* **2014**, *5*, 3949.
[7] W. T. Hong, M. Risch, K. A. Stoerzinger, A. Grimaud, J. Suntivich, Y. Shao-Horn, *Energy Environ. Sci.* **2015**, *8*, 1404.
[8] J. H. Wang, W. Cui, Q. Liu, Z. C. Xing, A. M. Asiri, X. P. Sun, *Adv. Mater.* **2016**, *28*, 215.
[9] H. F. Liang, F. Meng, M. Cabán-Acevedo, L. Li, A. Forticaux, L. Xiu, Z. C. Wang, S. Jin, *Nano Lett.* **2015**, *15*, 1421.
[10] J. Suntivich, K. J. May, H. A. Gasteiger, J. B. Goodenough, Y. Shao-Horn, *Science* **2011**, *334*, 1383.
[11] Y. W. Liu, H. Cheng, M. J. Lyu, S. J. Fan, Q. H. Liu, W. S. Zhang, Y. D. Zhi, C. M. Wang, C. Xiao, S. Q. Wei, B. J. Ye, Y. Xie, *J. Am. Chem. Soc.* **2014**, *136*, 15670.
[12] M.-R. Gao, Y.-F. Xu, J. Jiang, Y.-R. Zheng, S.-H. Yu, *J. Am. Chem. Soc.* **2012**, *134*, 2930.
[13] M.-R. Gao, X. Cao, Q. Gao, Y.-F. Xu, Y.-R. Zheng, J. Jiang, S.-H. Yu, *ACS Nano* **2014**, *8*, 3970.
[14] Y.-R. Zheng, M.-R. Gao, Q. Gao, H.-H. Li, J. Xu, Z.-Y. Wu, S.-H. Yu, *Small* **2015**, *11*, 182.
[15] K. Xu, P. Z. Chen, X. L. Li, Y. Tong, H. Ding, X. J. Wu, W. S. Chu, Z. M. Peng, C. Z. Wu, Y. Xie, *J. Am. Chem. Soc.* **2015**, *137*, 4119.
[16] D. H. Son, S. M. Hughes, Y. D. Yin, A. P. Alivisatos, *Science* **2004**, *306*, 1009.
[17] R. D. Robinson, B. Sadtler, D. O. Demchenko, C. K. Erdonmez, L.-W. Wang, A. P. Alivisatos, *Science* **2007**, *317*, 355.
[18] B. J. Beberwyck, Y. Surendranath, A. P. Alivisatos, *J. Phys. Chem. C* **2013**, *117*, 19759.
[19] X. Wu, Y. F. Yu, Y. Liu, Y. Xu, C. B. Liu, B. Zhang, *Angew. Chem. Int. Ed.* **2012**, *51*, 3211; *Angew. Chem.* **2012**, *124*, 3265.
[20] J. Zhang, J. G. Yu, Y. M. Zhang, Q. Li, J. R. Gong, *Nano Lett.* **2011**, *11*, 4774.
[21] G. D. Moon, S. Ko, Y. Xia, U. Jeong, *ACS Nano* **2010**, *4*, 2307.
[22] M.-R. Gao, W.-T. Yao, H.-B. Yao, S.-H. Yu, *J. Am. Chem. Soc.* **2009**, *131*, 7486.
[23] Y. F. Yu, J. Zhang, X. Wu, W. W. Zhao, B. Zhang, *Angew. Chem. Int. Ed.* **2012**, *51*, 897; *Angew. Chem.* **2012**, *124*, 921.
[24] C. E. M. Campos, J. C. de Lima, T. A. Grandi, K. D. Machado, P. S. Pizani, *Phys. B* **2002**, *324*, 409.
[25] H. Li, D. Gao, X. Cheng, *Electrochim. Acta* **2014**, *138*, 232.
[26] K. Samanta, P. Bhattacharya, R. S. Katiyar, W. Iwamoto, P. G. Pagliuso, C. Rettori, *Phys. Rev. B* **2006**, *73*, 245213.
[27] J. A. Tossell, D. J. Vaughan, J. K. Burdett, *Phys. Chem. Miner.* **1981**, *7*, 177.

[28] D. S. Kong, H. T. Wang, Z. Y. Lu, Y. Cui, *J. Am. Chem. Soc.* **2014**, *136*, 4897.
[29] J. Yang, G.-H. Cheng, J.-H. Zeng, S.-H. Yu, X.-M. Liu, Y.-T. Qian, *Chem. Mater.* **2001**, *13*, 848.
[30] D. C. Frost, C. A. McDowell, I. S. Woolsey, *Mol. Phys.* **1974**, *27*, 1473.
[31] H. Vanderherde, R. Hemmel, C. F. Vanbruggen, C. Haas, *J. Solid State Chem.* **1980**, *33*, 17.
[32] M. Romand, M. Roubin, J. P. Deloume, *J. Electron Spectrosc. Relat. Phenom.* **1978**, *13*, 229.
[33] Y. Gorlin, T. F. Jaramillo, *J. Am. Chem. Soc.* **2010**, *132*, 13612.
[34] C. Xia, Q. Jiang, C. Zhao, M. N. Hedhili, H. N. Alshareef, *Adv. Mater.* **2016**, *28*, 77.

Manuscript received: September 16, 2016
Revised: October 21, 2016
Final Article published: November 29, 2016

